Catalysis Today 177 (2011) 25–30

Contents lists available at ScienceDirect

Catalysis Today

journal homepage: www.elsevier.com/locate/cattod

A combined EXAFS and DFT study of the Ni^{2+} environment in dehydrated Ni/NaX

Hazar Guesmi, Pascale Massiani*

UPMC Univ Paris 06, Laboratoire de Réactivité de Surface, CNRS-UMR 7197, Site d'Ivry, Le Raphaël, 3 rue Gallilée, 94200 Ivry-sur-Seine, France

ARTICLE INFO

Article history:
Received 16 February 2011
Received in revised form 21 April 2011
Accepted 23 April 2011
Available online 31 May 2011

Keywords:
EXAFS
DFT
Nickel cation
Basicity
Zeolite faujasite

ABSTRACT

The location of the divalent nickel cation exchanged in low amount in dehydrated NaX is identified by a combination of experimental (XAS) and theoretical (DFT) approaches. The Ni–O and Ni–T distances as well as the coordination numbers evaluated from experiments are in good agreement with the predicted models obtained from calculations. After dehydration, the migration of Ni^{2+} towards the hexagonal prism is confirmed and three distinct possible nickel sites are predicted. The results show the tendency of Ni^{2+} to get closer to the most basic framework oxygen atoms.

1. Introduction

The location and environment of transition metal (TM) ions exchanged in zeolites, as well as the characteristics of the related metal–framework interactions, play an important role towards the active properties of such TM/zeolite heterogeneous catalysts. In order to achieve proper control of reactivity, studies devoted to the precise understanding of these parameters continue to deserve obvious interest. This is especially the case for Ni^{2+}-exchanged dehydrated faujasites (X and Y zeolites supports, with FAU structure [1]) that are active in reactions such as DeNOx [2–4], hydrogenation [5] or CO oxidation [6,7] but for which strong discrepancies are found in the literature regarding the Ni^{2+} coordination (from sixfold to threefold) and d_{Ni-O} distances (from more than 2.30 to less than 2.00 Å), depending on the study [8–22].

In hydrated Ni/faujasites, it is well established that the preferential location of Ni^{2+} is inside the supercages [9–12] that have pore diameters of the order of 13 Å [1], thus offering a space big enough to accommodate the nickel cation with its hydration sphere made of six water molecules. Upon complete dehydration, all H_2O ligands are removed and the Ni^{2+} ion migrates to more confined environments in order to optimize its coordination, being then stabilized by its interaction with the framework oxygen atoms, as classically occurs for ions in zeolites [19]. In the case of nickel, the preferred location – and even sole expected one when nickel is present in low content (few wt%) [15] – has been experimentally identified at site I [11–16], usually recognized as being at the centre of the hexagonal prism. In such position, average Ni–O distances between 2.21 and 2.37 Å with a coordination number of 6 were evaluated from XRD Rietveld refinements [11,15,23]. Nevertheless, it was latter noted that this distance could have been overestimated – a value of 2.16 Å being more probable – due to the fact that XRD gives a long range average information (including Ni-free crystal parts). Moreover, at the local level, a shift of 0.5 Å of all six O(3) oxygens around each Ni^{2+} cation towards the centre of the double six-member ring was reported [8,13]. Smaller Ni–O distances (from 1.87 to 2.05 Å) were also determined by EXAFS (extended X-ray absorption fine structure) for dehydrated Ni/Na-faujasite samples [13,18,24].

An interesting specificity of EXAFS for the study of TM exchanged zeolites is the ability of this technique to provide local information on the nature of the atomic neighbours, coordination number and bond lengths around the transition metal ion. Especially, we were able in a previous work [17] to follow by dispersive EXAFS the progressive changes, upon rehydration, of the Ni environment in a Ni/NaX zeolite (NaX being the common denomination of faujasite with atomic Si/Al ratio in the range 1.2–1.4). After dehydration, not only Ni–O but also Ni–T (T = Si, Al) linkages were identified, confirming the strong interaction between nickel and the zeolite framework. Moreover, d_{Ni-O} and d_{Ni-T} distances were measured, which interestingly suggested a location of the Ni ions distinct from the centre of the prisms, nickel being rather positioned closer to a part of the zeolitic lattice walls [17]. However, the exact position of nickel could not be reached from EXAFS data alone. Then, completing this experimental knowledge by theoretical calculations able to provide minimum energy configurations of Ni sitting offers a fruitful manner to reach a precise understanding of the sites. Such combination would reinforce the validity of sites description, the experimental and theoretical approaches

* Corresponding author.
E-mail address: pascale.massiani@upmc.fr (P. Massiani).

0920-5861/$ – see front matter © 2011 Elsevier B.V. All rights reserved.
doi:10.1016/j.cattod.2011.04.047

supporting each other. This is the purpose of this paper in which experimental (EXAFS) and theoretical (DFT) methods are applied in a complementary manner to clarify the sitting of Ni^{2+} inside the hexagonal prism of dehydrated Ni/NaX. Experimental data concerning the hydrated sample are also given for the sake of comparison. Moreover, only the case of a sample with low Ni content is considered in order to ensure nickel location inside the hexagonal prisms (known as the preferred location after dehydration [15]).

2. Experimental

2.1. Sample preparation

The Ni/NaX sample, with unit cell formula $Ni_{7.3}Na_{67}H_{0.4}Al_{82}Si_{110}O_{384}$ (Si/Al = 1.34) as deduced from atomic absorption (measurement made in the Chemical Analysis Centre of CNRS, Solaize, France) was prepared by refluxing a parent NaX zeolite (Union Carbide) for 24 h at 343 K in a diluted $Ni(NO_3)_2$ aqueous solution (<0.1 M, pH = 6.5). The sample was subsequently washed three times with distilled water, recovered by centrifugation and dried in air at 333 K. A part of the solid, containing 2.6 wt% Ni, was kept in room atmosphere (hydrated sample), whereas another part was dehydrated at 773 K in vacuum ($\approx 5 \times 10^{-5}$ Pa) during 30 min and sealed in a glass ampoule to avoid rehydration (dehydrated sample).

2.2. X-ray absorption spectroscopy (XAS)

The XAS spectra were collected at the Ni K-edge (8333 eV) on the Dispersive XAS beamline D11 of LURE synchrotron (Orsay, France). The hydrated and dehydrated samples were studied in the form of pressed wafers, placed in the latter case into a cell with controlled water-free N_2 atmosphere sealed with Kapton windows, which ensured absence of rehydration. For registration of the spectra recorded in the transmission mode at room temperature, the polychromatic white X-ray beam issued from the DCI storage ring (1.85 GeV, 250 mA) was reflected on a bent rectangular shaped Si(1 1 1) crystal that permitted to simultaneously delimit the used energy range and to focus this beam onto the sample. Detection of the signal was then obtained by collecting the transmitted divergent beam on a CDD camera, as detailed earlier [17]. The absorption was defined by $\ln(I_0/I)$ where I_0 and I are the incident and transmitted signals, respectively. The EXAFS signals ($k\cdot\chi(k)$) were extracted by standard procedures, using the Michalowicz's software package [26,27]. The Fourier transforms (FT) of the $w(k)\cdot\chi(k)\cdot k^3$ data were carried out in the range 2.0–11.3 $Å^{-1}$ ($w(k)$ is a Kaiser–Bessel window with a smoothness parameter of 3). The simulations of spectra were performed by FT filtering in the 1.1–3.5 Å range and by multiple-shell quantitative fitting using Ni–O and Ni–Si (or Ni–Al) back-scattering pairs. The phase and amplitude functions were calculated using FEFF 7.02 starting from the crystal structures of $Ni(NO_3)_2{\cdot}6H_2O$ and Ni_2SiO_4. Note that we checked that no Ni–Ni back-scattering pairs were present; indeed attempts made by including them resulted in simulations that were not successful, thus ensuring that such bonds are absent in our samples.

2.3. Cluster model

A Ni/NaX cluster made of 117 atoms ($H_{24}O_{60}Ni_1Na_8Al_{10}Si_{14}$) was considered for DFT calculations. This cluster, representing an extended hexagonal prism of faujasite with Si/Al ratio of 1.4, was obtained after optimizing the Ni-free Na-faujasite cluster previously built according to the following procedures (more details are available elsewhere [28]). First, the chemical composition $Si_{96}Al_{96}Na_{96}O_{384}$ of the LSX (Si/Al = 1) unit cell was considered. The distribution of the extra-framework cations among the different crystallographic sites was modelled by selecting the distribution defined by Viatle et al. [29] that corresponds to 32 ions in site SI′ within the sodalite cages facing the 6-membered rings (6-mr) of hexagonal prisms, 32 Na^+ in site SII facing the 6-mr of sodalite cages towards the supercages, and 32 extra cations in site SIII in the plane of the 12-ring (12-mr) windows (see Fig. 1 for sites positions). The second step consisted of cutting out, from the above Na-LSX zeolite lattice, a cluster of 120 atoms, $H_{24}O_{60}Na_{12}Al_{12}Si_{12}$, representing the hexagonal prism and a part of its environment. The third step was achieved by adjusting the Si/Al ratio of the cluster to 1.4 by replacing two Al sites by Si sites, thus giving the host NaX cluster that is characterized by a succession of AlO_4 and SiO_4 tetrahedra except for two sites in which Si atoms replace Al ones. These two Al/Si substitutions were made as follows. The first one was done in one of the two 6-membered ring (6-mr) of the hexagonal prism, the other 6-mr being kept untouched in order to provide the atomic Si/Al ratio of 1.4 (5 Al and 7 Si) in the prism. The second substitution was made outside the prism and it was positioned in a cluster part close to the substituted 6-mr (upper part of the cluster in Fig. 1c). After that, the number of sodium cations was adjusted to ensure charge neutrality and Ni^{2+} was introduced within the prism by replacing the two Na^+ located in I′ sites. Finally, all dangling bonds were saturated with H atoms (OH terminations set to 1.0 Å and orientated towards the direction of the next tetrahedral site) [28]. In the following, we denote 6-mr(3Al) and 6-mr(2Al) the six-rings forming the hexagonal prism and containing 3 and 2 Al atoms, respectively.

2.4. DFT calculation method

All density functional theory (DFT) calculations were performed using the Gaussian 03 package. Geometry optimizations were carried out using the Becke3–Lee–Yang–Parr (B3LYP) [30,31] hybrid functional. Basis sets at the 6-31G* level were used for the Si, Al, O, Na and H atoms. Ni was described using the extended 6-311+G* basis set. The same theoretical level was applied for the optimization of the $[Ni(H_2O)_6]^{2+}$ molecule and gave a d_{Ni-O} distance value of 2.06 Å, in fair agreement with the experimental bonds lengths reported for Ni–$(OH_2)_6$ in hydrated faujasites (2.04–2.06 Å) [13,17,18]. The B3LYP functional has proven to be effective for a number of transition metals exchanged in zeolites [32–34]. As shown in benchmark tests [35], when combined with the 6-31G* basis set, the DFT (B3LYP) appears to be the most accurate method for predicting reliable energies and bond lengths (10 kcal/mol and 0.03 Å, respectively). All geometries were optimized with an energy convergence criterion of at least 10^{-7} Ha and a maximum norm of the Cartesian gradient of 10^{-4} Ha/Bohr. No corrections were made with respect to the basis set superposition error (BSSE) [36]. During optimization, all atoms were allowed to relax except for the H terminations that were kept frozen. These fixed hydrogen atoms were positioned over the third coordination sphere of the hexagonal prism; far enough to consider the absence of effect of constraints that can be a source of artifacts in the cluster approach [37]. At the initial stage, a set of single-point energy calculations was performed to determine the spin state of nickel in the cluster. The single-point energies were calculated with different values of spin multiplicity and the lowest energy spin state was used for the subsequent calculations. Geometry optimization of Ni^{2+} interactions with framework faujasite was performed after calculating successive potential energy profiles (PES). For each calculation, the nickel was first located at a selected coordinate and a scan of the potential energy surface was applied along the z-axis. The resulting energy profiles with different basins (two examples are shown in Fig. 2) were used to localize the equilibrium geometries of nickel. Then, the geometry for each basin minimum energy configuration was re-optimized by means of EG calculations to obtain the final

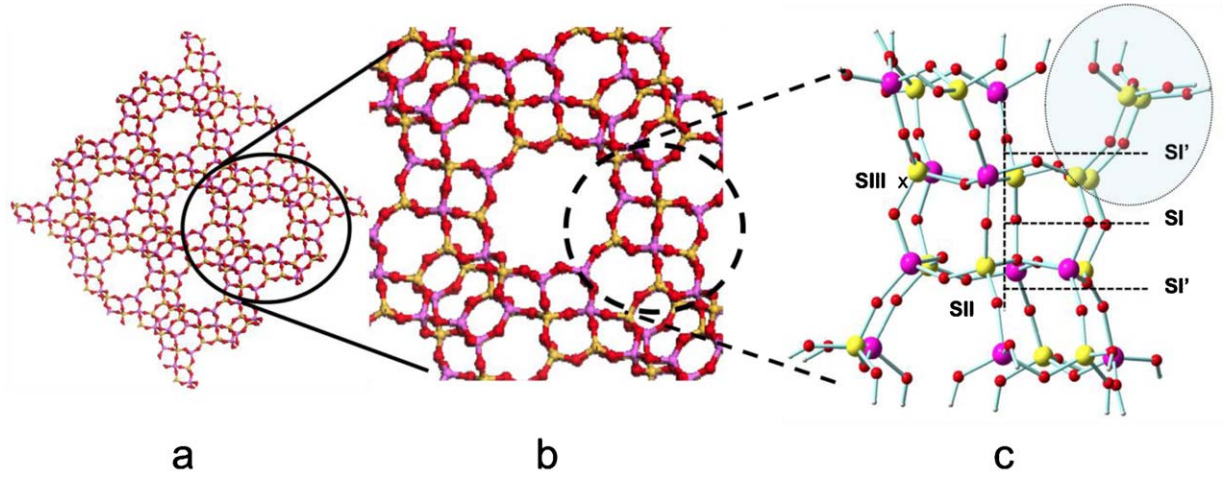

Fig. 1. Schematic representation at different levels of the faujasite (FAU) structure showing (a) the framework and pore system, (b) the unit cell and (c) the extended hexagonal prism with its classically referenced cationic site positions. The circle in (c) represents the anisotropic cluster part where two Si atoms substitute two Al atoms. The red, yellow and purple balls represent the oxygen, silicon and aluminium atoms, respectively. Hydrogen terminations are shown (in c) by small white balls. (For interpretation of the references to color in this figure legend, the reader is referred to the web version of the article.)

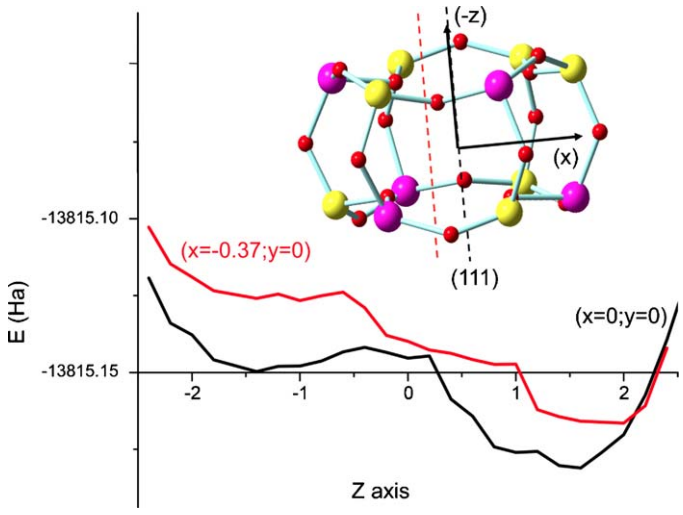

Fig. 2. Graph representing two scans of potential energy surface (PES) for nickel along the *z*-axis, with nickel being first positioned at two selected coordinates ((0,0,0) and (−0.37,0,0)); resulting curves showing the different basins of the energy profiles.

geometry for the particular location. In this last step of re-optimization calculation, the nickel coordinate was no longer fixed. Note that all the Ni/Na-FAU configurations considered in this paper as well as their related Ni–O and Ni–T distances correspond to such final equilibrium geometries. Moreover, for the evaluation of both the coordination numbers and the average d_{Ni-O} values, only the close oxygen atoms at d_{Ni-O} distances below 2.5 Å are considered; similarly, only the d_{Ni-T} distances below 4.0 Å are taken into account. Finally, Natural Bond Orbital (NBO) analysis was used to estimate oxygen Mulliken charges and electronic structures of nickel.

3. Results and discussion

3.1. Experimental study of the Ni^{2+} neighbouring in hydrated and dehydrated Ni/NaX

The EXAFS signal of hydrated Ni/NaX and its relative Fourier transformed spectrum are shown in Fig. 3a and b, respectively. The single shell visible in the FT spectrum corresponds to oxygen neighbours. Its spectral simulation leads to an average Ni–O bond distance of 2.06 Å and a coordination number of 6 (Table 1). Such values are typical of nickel hexacoordinated to oxygen atoms in the $Ni(H_2O)_6^{2+}$ complex, as is expected to be formed in the faujasite supercages in presence of hydration water. Moreover, the low value of the Debye–Waller factor (Table 1) indicates a strong symmetry and homogeneous Ni–O distances.

After dehydration, the EXAFS signal is significantly modified (Fig. 3a) and two FT contributions are identified (Fig. 3c), which reveal the presence of at least two ligand shells. The shell at the lower distance in the FT window is still attributable to oxygen neighbours, but it is slightly shifted and an intensity loss is observed, suggesting a decrease of coordination. This is indeed confirmed by the best fit for the simulation of this O shell that leads to a coordination number of about 5.5 and an average Ni–O distance of 2.11 Å (Table 1). Moreover, the value of the Debye–Waller factor, higher than above, reveals a larger disorder, which is in line with the symmetry loss expected if Ni^{2+} interacts no longer with water molecules but rather with the more rigid lattice environment.

Table 1
Interatomic Ni–O and Ni–T distances (R), number of neighbour oxygen and tetrahedral (Si, Al) atoms (N), and Debye–Waller factor (σ) obtained from spectra simulations for dehydrated and rehydrated Ni/NaX.

	Ni–O			Ni–T		
	R^a (Å)	N^b	σ (Å)	R^a (Å)	N^b	σ (Å)
Hydrated	2.06	6.0	0.08	–	–	–
Dehydrated	2.11	5.5	0.11	2.73	0.5	0.07
				3.33	4.0	0.07

[a] ±0.02.
[b] ±0.5.

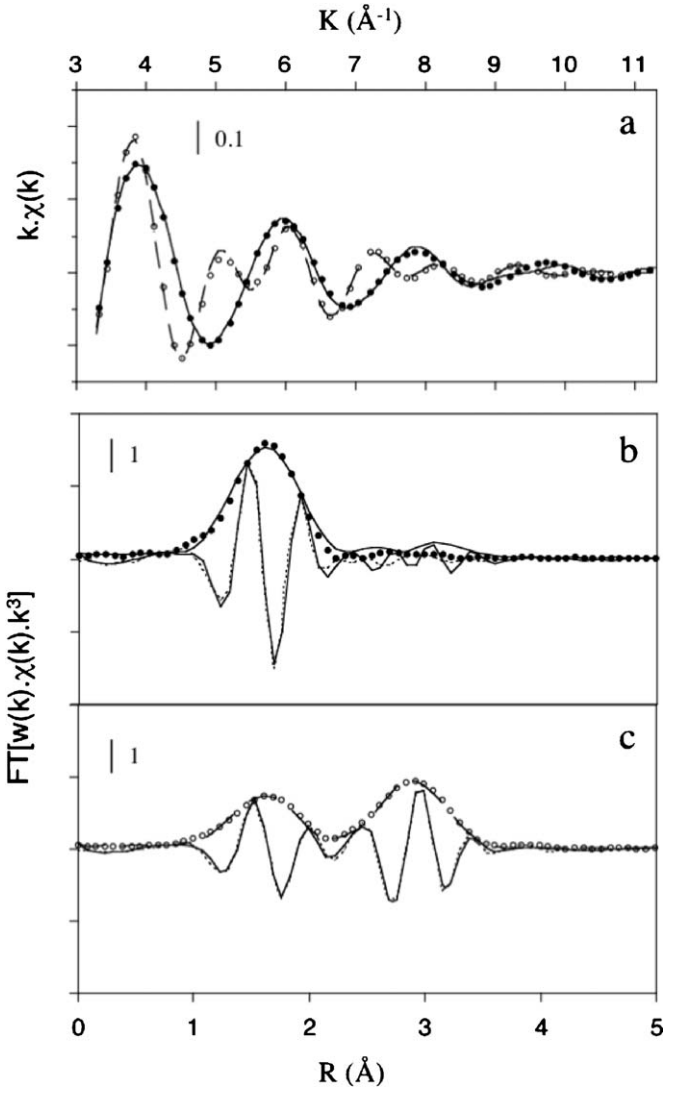

Fig. 3. (a) XAS spectra and (b and c) modulus of Fourier transform (FT) of the $w(k)\cdot\chi(k)\cdot k^3$ signals (reported before phase shift correction) at the Ni K-edge: experimental (dashed and full lines) and simulated (○,●) spectra for hydrated (dashed line, ○) and dehydrated (full line, ●) Ni/NaX. The good fit between the experimental (full line) and simulated (dashed lines) imaginary parts of the FT is also shown for (b) hydrated and (c) dehydrated Ni/NaX.

Besides this first shell, the most interesting new features are obtained from the second shell, which best simulation is obtained by assuming the presence of two sub-shells made of tetrahedral framework atoms (T = Si, Al), located at Ni–T distances of 2.73 and 3.33 Å, respectively (Table 1). Such spectral identification of the framework tetrahedral T neighbours attests of the narrow interaction that takes place between the Ni^{2+} cation and the zeolite lattice. It gives access to an accurate experimental knowledge on the nature and number of neighbour atoms and on bond distances around the nickel ion. This information is fruitfully used below to validate the site predictions available from calculations.

3.2. DFT predicted Ni^{2+} sitting in the hexagonal prism of Ni/NaX

DFT results considering nickel in its triplet state are reported hereafter. The geometry optimization of the Ni/NaX studied cluster predicts not solely one but three distinct possible Ni^{2+} locations, one being to some extent energetically less favorable ($\Delta E = 2.6$ kcal mol^{-1}) than the two others, as is illustrated in Fig. 4. For each configuration, the figure shows a "side" view and an "upper" view of the hexagonal prim, thus providing a detailed representation of the nickel location. Moreover, the values of the Ni–T (see side views) and Ni–O (see upper views) bond distances evaluated in each model are indicated.

The three distinct positions having slightly different stability levels can be discussed in view of the chemical anisotropy that exists in the hexagonal prism of the NaX cluster, in which one of the two six-membered rings is Al-richer than the other one. The most stable configuration is found for nickel stabilized in the plane of the 6-mr(3Al), where it can interact with four lattice oxygen atoms of the ring (three and one oxygens in O3 and O2 positions, respectively) through short bonds having lengths in the range 1.96–2.13 Å (site $SI'_{6\text{-mr(3Al)}}$, Fig. 4a). The average Ni–O distance for this fourfold coordinated site is 2.05 Å. Besides, two different ranges of d_{Ni-T} distances are found, being either below 3 Å (2.84 and 2.92 Å) or above 3.3 Å (four bonds with lengths between 3.34 and 3.42 Å). Noticeably, such Ni–O and Ni–T distances are also identified in the less stable configuration, with Ni^{2+} located in the plane of the 6-mr(2Al) (site $SI'_{6\text{-mr(2Al)}}$, Fig. 4c). Therefore, the Si-richer (Al-poorer) environment in this ring, which is known to decrease the basicity of the lattice oxygen neighbours [38], is seen to have only a small influence on the Ni position and on Ni–O and Ni–T bond distances; the effect of this lower basicity would rather be to slightly weaken the Ni^{2+} interaction with the framework (lower stability). In the third stable configuration (Fig. 4b), Ni^{2+} is found to be fivefold coordinated in a site hereafter denoted $SI_{Ni/NaX}$, positioned inside the hexagonal prism but shifted by 0.23 Å from the conventional

Table 2
Mulliken charges of the oxygen atoms and nickel electronic configurations in the three different Ni^{2+} sittings inside the NaX hexagonal prism.

Site	d_{Ni-O} (Å)	Oxygen Mulliken charges	Ni electronic configuration
$SI_{Ni/NaX}$	2.05	−0.901	[core]4S(0.23)3d(8.17)5S(0.01)
	2.19	−0.901	
	2.21	−0.860	
	2.42	−0.853	
	2.45	−0.799	
$SI'_{6\text{-mr(3Al)}}$	1.95	−0.883	[core]4S(0.31)3d(8.17)
	1.96	−0.890	
	2.07	−0.870	
	2.13	−0.868	
$SI'_{6\text{-mr(2Al)}}$	1.98	−0.900	[core]4S(0.29)3d(8.16)
	2.03	−0.892	
	2.06	−0.880	
	2.11	−0.837	

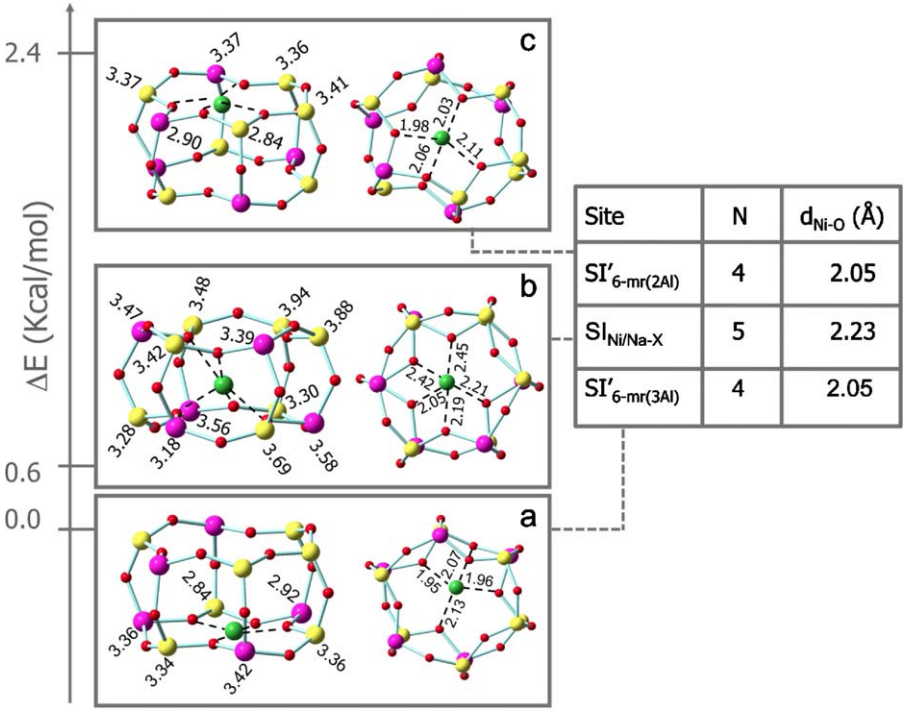

Fig. 4. DFT predicted Ni^{2+} sites in the hexagonal prism of dehydrated Ni/NaX and relative configuration stability (ΔE) with respect to the most stable configuration for Ni/NaX. The green, red, yellow and purple balls represent the nickel, oxygen, silicon and aluminium atoms, respectively. For each configuration, a side view and an upper view are presented, on which the values of all Ni–T (<4.0 Å) and Ni–O (<2.5 Å) distances, respectively, are indicated. The site denomination, Ni^{2+} coordination number (N) and average d_{Ni-O} distances are also reported. (For interpretation of the references to color in this figure legend, the reader is referred to the web version of the article.)

centered SI site towards the high Al content region (Fig. 4b). As compared to above, Ni^{2+} in such location can increase its coordination to a higher number of lattice oxygen atoms (2 and 3 oxygen atoms at O3 positions in the upper and bottom 6-mr, respectively). At the same time, the Ni–O bond lengths are significantly increased, being in the range 2.05–2.45 Å, and only Ni–T distances above 3.1 Å are found. Therefore, the higher the coordination numbers of nickel, the longer the Ni–O bond. This compromise between coordination number and bond length leads to a configuration that is found energetically competitive (ΔE = +0.6 kcal mol^{-1}, Fig. 4) with respect to the most stable fourfold configuration in site $SI'_{6\text{-}mr(3Al)}$.

In Table 2 are reported the oxygen Mulliken charges and the nickel electronic configurations obtained from NBO analysis for the three equilibrium geometries. Even if the nickel configuration does not change significantly whatever its coordination (five or four), one can see that the d_{Ni-O} bound length tends to decrease when the charge of the bounding oxygen increases. This well illustrates the tendency of Ni^{2+} to get closer to the most basic framework oxygen atoms.

3.3. *Precise site description from combined experimental/theoretical methods*

As already stated above, the EXAFS technique has the advantage to identify at the experimental level the individual and instantaneous local structure around the nickel ion. In the present dehydrated Ni/NaX sample, it is especially able to detect the occurrence of two different ranges of Ni–T distances. This experimental information, as well as the other data available from spectral simulations, interestingly leads to Ni^{2+} environments that are in very good concordance with DFT optimized configurations.

In the hexagonal prism of the NaX faujasite, a competition between the fivefold (Ni^{2+} sitting near the centre of the hexagonal prism) and fourfold (Ni^{2+} sitting in the plane of the 6-mr) coordination is predicted. In all sites, the nickel tends to approach Al-rich regions, which illustrates its affinity for the most basic lattice oxygen atoms (connected to Al tetrahedra). Moreover, in the plane of the 6-mr, Ni^{2+} is close to the border of the faujasite wall, which induces noticeable local deformation of the 6-mr (upper views in Fig. 4a and c). The d_{Ni-Si} (2.84 Å) and d_{Ni-Al} (2.92 Å) distances predicted by DFT for Ni^{2+} in SI′ sites show the high agreement that exists between the present calculations and the EXAFS simulations that also reveals the occurrence of d_{Ni-T} values below 3.0 Å (Table 1). In addition, if we assume (i) that each of the sixteen hexagonal prisms of the faujasite unit cell is occupied by one Ni^{2+} and (ii) that all three DFT optimized positions exist in Ni/NaX, we can consider the Boltzmann energy distribution at 298 K, given by the equation $P_i/P_j = \exp(-\Delta E_{ij}/RT)$, where $\Sigma P_i = 1$. The following proportions of 1.4%, 26.6% and 72.0% are then deduced for nickel in sites $SI'_{6\text{-}mr(2Al)}$, $SI_{Ni/NaX}$ and $SI'_{6\text{-}mr(3Al)}$, respectively. Applying this distribution, we can evaluate a predicted Ni–O average bond length of 2.10 Å, which is in fair agreement with the Ni–O distance of 2.11 Å measured by EXAFS. From their study of the cation environment after dehydration of nickel exchanged zeolite, Dooryhee et al. [13] have proposed a similar average Ni–O bond value, which permitted to explain the discrepancy between XRD and EXAFS results. These authors have assigned such a short distance to nickel cations sitting in SI sites. Using the Diffuse Reflectance Spectroscopy technique, Le petit and Che [16] have demonstrated that such short distance lie out of the range of octahedral or distorted octahedral nickel species in SI site and should therefore be reassigned to four-coordinated cations in distorted tetrahedral symmetry located in SI′ sites, such proposal being in line with our findings.

4. Conclusion

In this work, the three distinct DFT predicted nickel sittings inside the hexagonal prism of a dehydrated Ni/NaX with low Ni content are confirmed owing to the information gained from EXAFS

experiments. Especially, the rather short average d_{Ni-O} distance evaluated by EXAFS, around 2.11 Å, as well as the occurrence of short d_{Ni-T} distances, below 3.0 Å, reveal that nickel is located not solely at a position close to the centre of the prism but also, for more than 70% of the Ni^{2+} ions, in the planes of the two 6-mr constitutive of the prism, as is predicted by calculations. Such a precise site description could not have been reached by applying the experimental approach alone. Similarly, the experiments are needed to validate the relevance of DFT predictions. This demonstrates the high power of combining experimental and theoretical approaches for the identification of TM sites in zeolites or more generally in heterogeneous catalysts.

Acknowledgements

This work was granted access to the HPC resources of [CCRT/CINES/IDRIS] under the allocation 2010 [x2010086395] made by GENCI (Grand Equipement National de Calcul Intensif). Françoise Villain, François Baudelet and the LURE synchrotron are sincerely acknowledged for their contribution to XAS experiments. Jean-François Groust is gratefully thanked for the Ni/NaX sample preparation.

References

[1] Ch. Baerlocher, L.B. McCusker, D.H. Olson, Atlas of Zeolite Framework Types, 6th revised edition, Elsevier, Amsterdam, 2007.
[2] M. Mihaylov, K. Hadjiivanov, D. Panayotov, Appl. Catal. B 51 (2004) 33.
[3] B.I. Mosqueda-Jimenez, A. Jentys, K. Seshan, J.A. Lercher, J. Catal. 218 (2003) 348.
[4] Y. Li, J.N. Armor, Appl. Catal. B 3 (1993) L1.
[5] S. Bhatia, J.F. Mathews, N.N. Bakhshi, Acta Phys. Chem. 24 (1978) 83.
[6] M. Suzuki, K. Tsutsumi, H. Takahashi, Y. Saito, Zeolites 9 (1989) 98.
[7] M. Sano, M. Suzuki, M. Niwa, Bull. Chem. Soc. Jpn. 66 (1993) 3511.
[8] D.H. Olson, J. Phys. Chem. 72 (1968) 4366.
[9] R.M. Haniffa, K. Seff, J. Phys. Chem. B 102 (1998) 2688.
[10] Y. Horikawa, N. Ohnishi, K. Hiraga, Mater. Sci. Eng. A217/218 (1996) 139.
[11] J.M. Thomas, C. Williams, T. Rayment, J. Chem. Soc., Faraday Trans. 1 84 (1988) 2915.
[12] Y. Sendoda, Y. Ono, T. Keii, J. Catal. 39 (1975) 357.
[13] E. Doorhyhee, C.R. Catlow, J.W. Couves, P.J. Maddox, J.M. Thomas, G.N. Greaves, A.T. Steel, R.P. Townsend, J. Phys. Chem. 95 (1991) 4514.
[14] M. Briend-Faure, J. Jeanjean, M. Kermarec, D. Delafosse, J. Chem. Soc., Faraday Trans. 1 74 (6) (1978) 1538.
[15] P. Gallezot, B. Imelik, J. Phys. Chem. 77 (1973) 652.
[16] C. Lepetit, M. Che, J. Phys. Chem. 100 (1996) 3137.
[17] J.F. Groust, C. Pommier, L. Stievano, F. Villain, C. Giorgetti, F. Baudelet, P. Massiani, Catal. Lett. 102 (2005) 257.
[18] M. Sano, T. Maruo, H. Yamatera, M. Suzuki, Y. Saito, J. Am. Chem. Soc. 109 (1987) 52.
[19] G.R. Eulenberger, D.P. Shoemaker, J.G. Keil, J. Phys. Chem. 71 (1967) 1812.
[20] K.C. Woong, K.J. Jung, N.H. Heo, S.H. Kim, S.B. Hong, K. Seff, J. Phys. Chem. C 113 (2009) 5164.
[21] M.A. Zanjanchi, A. Ebrahimian, Mater. Chem. Phys. 110 (2008) 228–230.
[22] C.J.J. Den Ouden, R.A. Jackson, C.R.A. Catlow, M.F.M. Post, J. Phys. Chem. 94 (1990) 5286–5290.
[23] A.R. George, C.R.A. Catlow, J.M. Thomas, Catal. Lett. 8 (1991) 193.
[24] H. Forster, U. Hatje, Solid State Ionics 101–103 (1997) 425.
[26] A. Michalowicz, Logiciels pour la Chimie, SFC, Paris, 1991.
[27] A. Michalowicz, Journal de Physique IV France 7 (1997) 235.
[28] H. Guesmi, D. Costa, D. Berthomieu, P. Massiani, J. Phys. Chem. C 115–13 (2011) 5607.
[29] G. Vitale, C.F. Mello, L.M. Bull, A.K. Cheetham, J. Phys. Chem. B 101 (1997) 4559.
[30] A.D. Becke, Phys. Rev. A 38 (1988) 3098.
[31] C. Lee, W. Yang, R.G. Parr, Phys. Rev. B 37 (1988) 785.
[32] F. Furche, J.P. Perdew, J. Chem. Phys. 124 (2006) 044103.
[33] D. Berthomieu, S. Krishnamurty, in: V.A. Basiuk, P. Ugliengo (Eds.), Quantum Chemical Calculations of Surfaces and Interfaces of Materials, American Scientific Publishers, Valencia, CA, 2009, pp. 107–132.
[34] H. Guesmi, D. Berthomieu, L. Kiwi-Minsker, Stud. Surf. Sci. Catal. 174 (2008) 1123.
[35] NIST Computational Chemistry Comparison and Benchmark Database, NIST Standard Reference Database Number 101, Release 12, Aug 2005 (Ed. Russell D. Johnson III).
[36] S.F. Boys, F. Bernradi, J. Mol. Phys. 19 (1970) 553.
[37] J. Sauer, D. Nachtigallova, P. Nachtigall, in: G. Centi, B. Wichterlova, A.T. Bell (Eds.), Catalysis by Unique Metal Ion Structures in Solid Matrices, vol. II/13, Kluwer Ed., 2001, p. 221.
[38] D. Barthomeuf, Catal. Rev. Sci. Eng. 38 (1996) 521.